Experimental cancellation of aberrations in intensity correlation in classical optics

A. J. Jesus-Silva,[1] Juarez G. Silva,[1] C. H. Monken,[2] and E. J. S. Fonseca[1,*]
[1]*Instituto de Física, Universidade Federal de Alagoas, Maceió, AL, 57061-970, Brazil*
[2]*Departamento de Física, Universidade Federal de Minas Gerais, Caixa Postal 702, Belo Horizonte, MG 30123-970, Brazil*

(Received 19 May 2017; revised manuscript received 26 July 2017; published 22 January 2018)

We study the classical correlation function of spatially incoherent beams with a phase aberration in the beam path. On the basis of our experimental measurements and in the optical coherence theory, we show that the effects of phase disturbances, independently of their kind and without need of coordinate inversion, can be canceled out if the same phase is aligned in the signal and reference beam path. These results can be useful for imaging and microscopy through random media.

DOI: 10.1103/PhysRevA.97.013832

I. INTRODUCTION

Optical systems may cause distortions of the light, the so-called aberrations [1]. They can be chromatic aberrations, an effect resulting from dispersion due to the impossibility to focus all colors to the same point, or monochromatic aberrations, where the rays emerging from one object point O will not all meet at a single image point O'.

The field of correlated-photon imaging with cancellation of aberrations has been a fairly active research line [2–11]. The first steps in this direction started with the measurements of dispersion cancellation using entangled two-photon beams generated by the process of spontaneous parametric down-conversion (SPDC) [2,3], which found applications in clock synchronization [4] and in quantum-optical coherence tomography [5]. Another direction was the use of correlated-photon imaging for the cancellation of phase aberrations [6,7] with applications in correlation confocal microscopy [8] and in cancellation of atmospheric turbulence effects [9,10]. Particularly, a recent work detailed the conditions under which the cancellation of aberrations in entangled two-photon beams takes place [11]. The authors demonstrated the cancellation of odd-order aberrations in correlated-photon imaging using entangled photons generated via SPDC, where the method of cancellation relies on a coordinate inversion of one of the entangled photons.

It is worthwhile to mention that demonstrations of dispersion cancellation using classical light with interferometry [12] and intensity correlation [13] were studied as well. One of the approaches to the study of light intensity correlation for imaging is based on the so-called ghost-imaging scheme [14]. Thanks to an analogy between the quantum and classical intensity light correlations the studies of ghost imaging from the classical viewpoint have been very fruitful [15,16]. Some authors have suggested theoretical models for the cancellation of phase aberrations using classical light in the ghost-imaging scheme [17,18]. However, a detailed experimental study of the cancellation of phase aberrations using classical light intensity correlation is still missing.

In this paper, we show that when exploring the correlations of fluctuations in speckle intensity it is possible to cancel out aberrations that may exist in the Fraunhofer plane of an optical system. The aberration cancellation occurs independently of its shape and it does not need coordinate inversion. Therefore, we extended the quantum-classical analogy to the study of cancellation of phase aberrations showing an interesting and useful distinction from the quantum case [11]. It is possible to embed images into speckle patterns which, through the spatial correlation function, can be recovered [19]. Images also can be recovered from the spatial intensity autocorrelation through the Fienup's phase retrieval algorithm [20–22]. Therefore, this effect can be useful in imaging through random media and microscopy, where inherent aberrations causing distortions in the image can be canceled.

II. EXPERIMENTAL SETUP

The experimental setup is shown schematically in Fig. 1. An argon ion laser is transmitted through a rotating ground glass disk (RGGD) producing a partially coherent Gaussian beam. Two lenses, L_1 and L_2, with $f_1 = 30$ mm and $f_2 = 500$ mm of focal length, were used to control the source size and to collimate the speckles, respectively. It is possible to control the coherence length δ at the plane of a double slit A, by adjusting the distance between the lens L_1 and the RGGD [23]. A double slit of slit width $a = 0.25$ mm and spacing $d = 0.45$ mm was placed immediately after lens L_2. The double slit is imaged over the spatial light modulator (SLM) by two $4f$-configuration systems formed by lens L_3 confocal with L_5, and L_4 confocal with L_5, with $f_i = 300$ mm, $i = 3, 4$, and 5. The beams that pass through L_3 and L_4 are the reference and signal beams, respectively. Using a beam blocker we can choose one of two paths: the red, which is horizontally inverted (I) in relation to the reference beam or the yellow, which is horizontally noninverted (NI) in relation to the reference beam. For simplicity, we have defined one-dimensional polynomial monochromatic wave aberrations of the form $\psi_n(x) = \pi(x/\alpha)^n$, where α is a constant that express the strength of the

*eduardo@fis.ufal.br

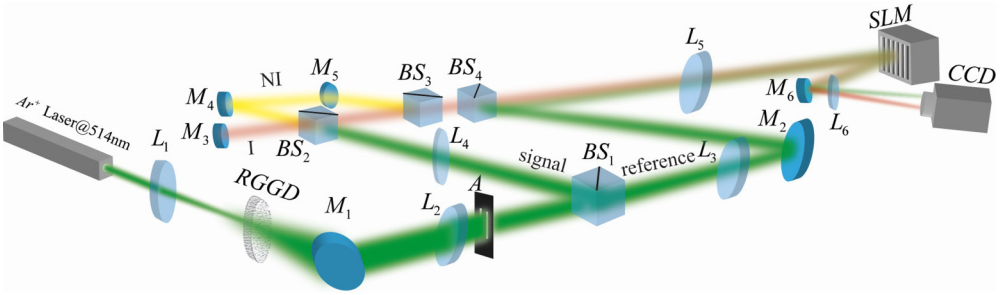

FIG. 1. Experimental setup: $M_1 - M_6$ are mirrors, $L_1 - L_6$ are lenses, $BS_1 - BS_4$ are beam splitters, RGGD is a rotating ground glass disk, A is a double-slit aperture, SLM is a spatial light modulator, and CCD is a charge-coupled (CCD) camera. Polynomial aberrations of the form $\psi_n(x) = \alpha_n x^n$ ($n = 1,2,3,4$) and a random phase are displayed on the SLM. I and NI stand for inverted and noninverted beams, respectively.

aberrations [11]. To give an example of a two-dimensional and arbitrary wave aberration we also have defined a random phase (RP) aberration. These aberrations are imprinted in the beam wave front using the SLM. Inverting the beam actually results in a coordinate inversion of the phase aberration.

The optical Fourier transform of the SLM plane is projected over a charge-coupled device (CCD) camera by a lens L_6 of $f_6 = 250$ mm. The signal and reference beams are projected in two different sections of the CCD area, but they illuminate the same region of the SLM display.

III. THEORY

Let $E_S(\mathbf{x}_S,t)$ and $E_R(\mathbf{x}_R,t)$ be spatially stochastic electromagnetic fields in the scalar and monochromatic approximations. We consider $\mathbf{x}_i = (x_i, y_i)$ the transversal coordinates and $i = S,R$ stands for signal and reference beams, respectively. The intensities are given by $I_i(\mathbf{x}_i) = |E_i(\mathbf{x}_i,t)|^2$. We have calculated the second-order spatial intensity correlations using the definition [24]

$$G^{(2,2)}(\mathbf{x}_S,\mathbf{x}_R) = \langle I_S(\mathbf{x}_S) I_R(\mathbf{x}_R)\rangle, \tag{1}$$

where $\langle\cdots\rangle$ means ensemble average. The coordinates $\mathbf{x}_S$ and $\mathbf{x}_R$ in Eq. (1) refer to different detection planes, as represented in Fig. 2. The speckle patterns shown were shifted from the center due to a linear phase aberration.

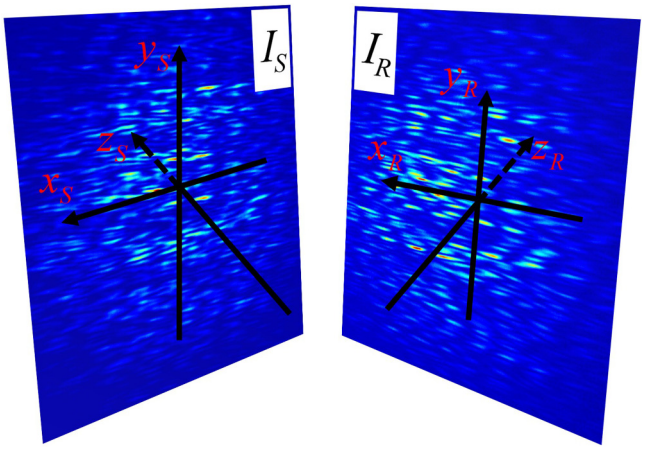

FIG. 2. Detection planes for S and R intensities in Eq. (1).

Defining the ensemble average of the intensities as $\bar{I}_i(\mathbf{x}_i) = \langle E_i^*(\mathbf{x}_i,t) E_i(\mathbf{x}_i,t)\rangle$, the normalized first-order correlation function can be written as

$$g(\mathbf{x}_S,\mathbf{x}_R) = \frac{G^{(1,1)}(\mathbf{x}_S,\mathbf{x}_R)}{\sqrt{\bar{I}_S(\mathbf{x}_S)\bar{I}_R(\mathbf{x}_R)}} = \frac{\langle E_S^*(\mathbf{x}_S) E_R(\mathbf{x}_R)\rangle}{\sqrt{\bar{I}_S(\mathbf{x}_S)\bar{I}_R(\mathbf{x}_R)}}. \tag{2}$$

Assuming Gaussian statistics, the Reed's momentum theorem [25] can be employed to relate the spatial intensity correlation, Eq. (1), to the field correlations, Eq. (2),

$$G^{(2,2)}(\mathbf{x}_S,\mathbf{x}_R) = \bar{I}_S(\mathbf{x}_S)\bar{I}_R(\mathbf{x}_R)[1 + |g(\mathbf{x}_S,\mathbf{x}_R)|^2]. \tag{3}$$

According to Eq. (3) the intensity correlation function is the first-order correlation function plus a background. Therefore, we are considering the propagation of the first-order correlation function from the SLM to the CCD camera, once the double-slit plane was imaged over the SLM, and that the S and R fields were subjected to identical apertures $A(\mathbf{u}_i) = |A(\mathbf{u}_i)|$ with phase aberrations $\exp[i\phi(\mathbf{u}_i)]$. Let $G_0^{(1,1)}(\mathbf{u}_S,\mathbf{u}_R)$ be the first-order correlation at the SLM plane. Then we can calculate the first-order correlation function at the plane of the CCD camera as

$$\begin{aligned} G^{(1,1)}(\mathbf{x}_S,\mathbf{x}_R) = &\iint_\Omega |A(\mathbf{u}_S)||A(\mathbf{u}_R)| \exp[i\phi(\mathbf{u}_R) - i\phi(\mathbf{u}_S)] \\ &\times G_0^{(1,1)}(\mathbf{u}_S,\mathbf{u}_R) h^*(\mathbf{u}_S,\mathbf{x}_S) h(\mathbf{u}_R,\mathbf{x}_R) d\mathbf{u}_S d\mathbf{u}_R, \end{aligned} \tag{4}$$

where $h(\mathbf{u}_i,\mathbf{x}_i) = \exp[i\pi\mathbf{u}_i\cdot\mathbf{x}_i/(\lambda f_6)]$, and the integral is performed over all region Ω where it has non-negligible values. For small coherence length, the first-order correlation function at the SLM can be modeled by a Dirac's delta $G_0^{(1,1)}(\mathbf{u}_S,\mathbf{u}_R) = \delta(\mathbf{u}_R - \mathbf{u}_S)$ because $\bar{I}_i(\mathbf{x}_i)$ is approximately constant. Therefore, Eq. (4) becomes

$$\begin{aligned} G^{(1,1)}(\mathbf{x}_S,\mathbf{x}_R) &= \int_\Omega A(\mathbf{u}) \exp[i2\phi_\pm(\mathbf{u})] \\ &\quad\times \exp\left[\frac{i\pi}{\lambda f_6}\mathbf{u}\cdot(\mathbf{x}_R - \mathbf{x}_S)\right] d\mathbf{u} \\ &= \tilde{A}_\phi\left(\frac{\mathbf{x}_R - \mathbf{x}_S}{\lambda f_6}\right), \end{aligned} \tag{5}$$

where $\tilde{A}_\phi$ is the Fourier transform of the aperture and $\phi_\pm(\mathbf{u}) = [\phi(\mathbf{u}) - \phi(\pm\mathbf{u})]/2$, where the ϕ_+ corresponds to the configuration without horizontal inversion of the phase aberrations in the signal beam, i.e., the beam takes path NI, and ϕ_- corresponds

to the configuration with horizontal inversion of the phase aberrations in the signal beam; i.e., the beam takes path I. It is clear that aberrations are completely canceled, independently of its shape, for the noninverted configuration, i.e., $\phi_+ = 0$. For the inverted configuration, we have two times the effect of the antisymmetrical part of the phase aberration.

We also have calculated the mean cross-correlation [19,26] between the signal and reference intensities,

$$\Gamma(\mathbf{x}) = \left\langle \int_\Omega I_S(\mathbf{x}') I_R(\mathbf{x}' - \mathbf{x}) d\mathbf{x}' \right\rangle, \tag{6}$$

where $I_S(\mathbf{x})$ is the signal intensity and $I_R(\mathbf{x}' - \mathbf{x})$ is the reference intensity rotated of 180°, the symbol $\langle \cdots \rangle$ indicates the average, and Ω is the domain where the integral has nonvanishing values. Naturally, we can rewrite Eq. (6) as

$$\Gamma(\mathbf{x}) = \int_\Omega \langle I_S(\mathbf{x}') I_R(\mathbf{x}' - \mathbf{x}) \rangle d\mathbf{x}' = \int_\Omega G^{(2,2)}(\mathbf{x}', \mathbf{x}' - \mathbf{x}) d\mathbf{x}'. \tag{7}$$

For the δ-correlated model, we have $\bar{I}_S(\mathbf{x}) \cong \bar{I}_R(\mathbf{x}) \cong K$ constant, and Eqs. (2), (3), and (5) show that Eq. (7) becomes

$$\Gamma(\mathbf{x}) \propto K^2 + \left| \tilde{A}_\phi \left(\frac{\mathbf{x}}{\lambda f_6} \right) \right|^2, \tag{8}$$

showing that the in the second-order intensity cross-correlation the aberrations can also be canceled out.

The analogy between the classical and quantum intensity correlations is based on fact that the spatial pump field in the SPDC process plays the role of the source intensity distribution in the incoherent case and that two-particle wave function in the SPDC process is the analog to the second-order coherence function in the incoherent case. The entangled two-photon wave function can be written as [27]

$$\psi(x_1, x_2) = \int dx E_p(x) h_s(x_1, x) h_i(x_2, x), \tag{9}$$

where s, i refer to signal and idler beams and $E_p(x)$ is the pump field. At this point it is interesting to compare this equation with Eq. (4). The entangled two-photon wave function depends on the product of the impulse-response functions of the signal and idler beams. The product of these impulse-response functions contains the effect of the sum of the aberrations in the signal and idler beams [11]. Interestingly enough, this product, in Eq. (4), depends on the difference of the phase aberration of the signal and reference beams. We observe that, differently from the entangled two-photon case, Eq. (9), the phase aberrations are always canceled in Eq. (4) independently of its functional form.

IV. EXPERIMENTAL RESULTS

The procedure used to obtain the mean intensity correlation between the signal and reference speckle patterns was the following: We measured the reference intensity followed by the signal intensity, and we calculated the cross-correlation between them, which is the integral in Eq. (6). In this experiment, we have averaged over 80 measurements of the cross-correlation corresponding to different positions of the RGGD. After evaluating the mean intensity correlation, we have taken a profile at the center of the result.

By recording the speckle patterns' intensities at a plane immediately before the double slit, it is possible to obtain the coherence length at this plane by evaluating the intensity autocorrelation of these patterns. The full width at half maximum (FWHM) of a Gaussian fit of the autocorrelation gives the coherence length of $\delta = 0.06$ mm.

From this point on, all measurements were performed at the focal plane of L_6. Figures 3(a)–3(e) show the normalized intensity correlation profiles of $|\tilde{A}_\phi|^2$, for different phase aberrations, $\psi_n(x) = \pi(x/\alpha)^n$, for $n = 1,2,3,4$ and a RP, respectively. We have used $\alpha = 0.2$ mm for $n = \{1,3\}$ and $\alpha = 0.3$ mm for $n = \{2,4\}$. To obtain the $|\tilde{A}_\phi|^2$ we just performed a background subtraction [28]. In Fig. 3(f) we see the effect of subtracting the background.

To capture the intensity patterns of the signal or reference beams we have used matrices of 810×810 pixels of the CCD camera, corresponding to an area of 2.8 mm × 2.8 mm. The black curves (squares) are the nonaberrated results obtained from the intensity correlation between the signal and reference beams with $n = 0$. The red curves (circles) correspond to the correlation with horizontal inversion of the phase aberrations in the signal beam, path I. The blue curves (triangles) correspond to the correlation without horizontal inversion of the phase aberrations in the signal beam, path NI. We observe that for the NI path all the aberrations are canceled, in agreement with the theory presented in Sec. III. Nevertheless, in some cases, there is not a complete match with the nonaberrated curves. The origin of this mismatch is due to the finite coherence length as well as the value of the parameter α. For a finite coherence length, the reference and signal beams may be influenced by different phase aberration profiles. For a perfect aberration cancellation, independently of the phase aberration profile, we should have a truly delta-correlated field. In Sec. V, we will provide a better explanation of this point. We would like to note that for the case of using the NI path the correlation result is similar to an autocorrelation, because the signal and reference beams are the same.

The phase inversion does not affect even aberrations, Figs. 3(b) and 3(d), but it does effect odd aberrations, as can be clearly seen in Figs. 3(a) and 3(c). In Fig. 3(e), it was used a random phase aberration and we observe that, for path NI, the aberrations are canceled, since the maxima coincides with the maxima of the nonaberrated graph. For path I, the peaks are randomly positioned for each random phase and, therefore, the aberrations are not canceled.

In order to quantify the mismatch between aberrated and nonaberrated curves, we have applied the definition of the difference between two curves [11],

$$D = \frac{1}{2} \sum_j |\Gamma^{\text{aber}}(x_j) - \Gamma^0(x_j)|, \tag{10}$$

where Γ^{aber} is the normalized aberrated correlation curve and Γ^0 is the normalized nonaberrated curve. This quantity varies from 0 (maximum overlap) to 1 (completely disjoint curves). The results for D, calculated from the same data used to obtain Fig. 3, are shown in Table I, where D^{I} and D^{NI} refer to the configuration with and without inversion of the coordinate of

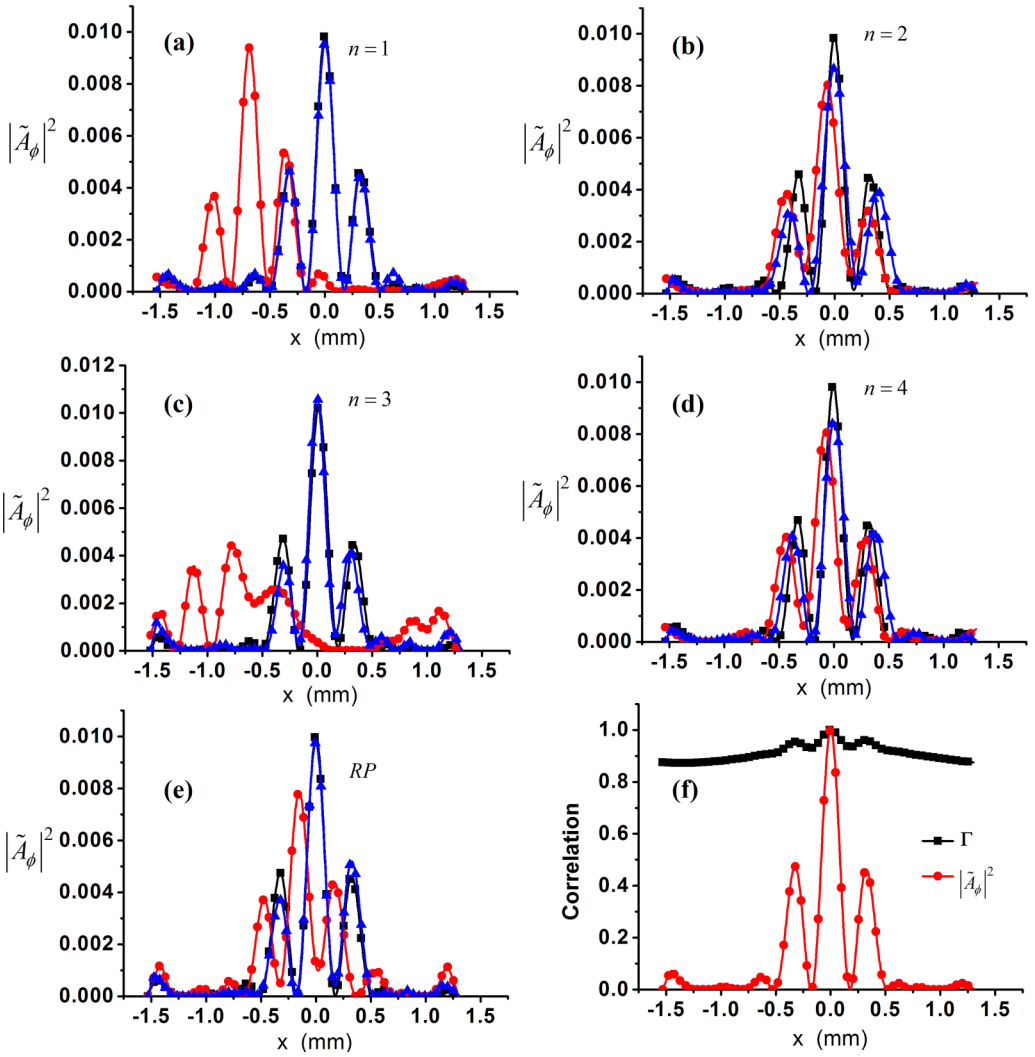

FIG. 3. (a–e) Measured high-order normalized (by its sum) intensity correlation profiles for $\delta = 0.06$ mm for different phase aberrations. Black (squares): nonaberrated curve for the case without aberrations in the SLM. Red circles: aberrated curves with coordinate inversion of the phase of the signal beam. Blue triangles: corrected curves (without coordinate inversion of the phase of the signal beam). (f) Comparison between the correlation with $|\tilde{A}_\phi|^2$ and without background subtraction Γ.

the phase of the signal beam, respectively. We also defined the relative differences due to coordinate inversion,

$$r_D = (D^{\mathrm{I}} - D^{\mathrm{NI}})/D^{\mathrm{I}}. \tag{11}$$

TABLE I. Deviation of aberrated curves without and with coordinate inversion (D^{NI}, D^{I}) from the nonaberrated and relative difference due to coordinate inversion of the phase of the signal beam. The symbol $\sim$0 is used for values smaller than the error. These results correspond to the coherence length of $\delta = 0.06$ mm.

	D^{NI}	D^{I}	$r_D(\%)$
$n = 1$	0.15 ± 0.03	0.70 ± 0.03	78 ± 7
$n = 2$	0.27 ± 0.04	0.19 ± 0.03	$\sim$0
$n = 3$	0.22 ± 0.05	0.66 ± 0.04	67 ± 10
$n = 4$	0.22 ± 0.04	0.16 ± 0.03	$\sim$0
RP	0.17 ± 0.03	0.40 ± 0.05	58 ± 16

The error is the standard deviation of the mean. This error could be reduced by increasing the area of the CCD camera illuminated by the speckles. The symbol $\sim$0 means that the value obtained for r_D should be zero. Notice that for the RP aberration we have obtained $D^{\mathrm{I}} = 0.40 \pm 0.05$, which is not as large as the values obtained for odd-order aberrations. This happens because every function can be written as a sum of an odd function and an even function. Therefore, according to our previous discussion the even part will be canceled but the odd part is not canceled with inversion of the coordinate of the phase of the signal beam. Therefore, due to the random character of the phase, the value for the distance D^{I} and of r_D also fluctuates randomly, and for another random phase the value for r_D could have another larger value.

V. SIMULATION

We have observed that in general there is not a perfect phase aberration cancellation. Therefore, the present simulation clarifies some effects of the coherence length δ, and shows what

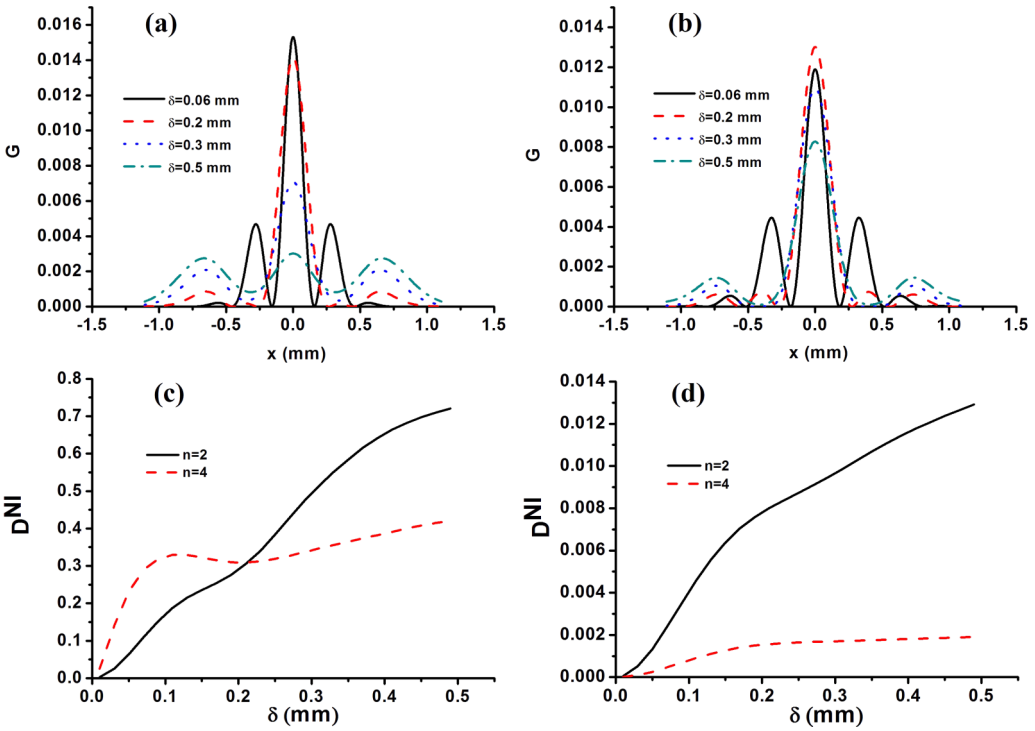

FIG. 4. Simulation results of the first-order correlation curves for the noninverted configuration where a complete aberration cancellation is expected, (a) $n = 2$ and (b) $n = 4$; simulation results of the difference between the aberrated and nonaberrated first-order correlation curves varying the coherence length δ for $\alpha = 0.3$ mm (c) and $\alpha = 0.8$ mm (d).

kind of results should be expected for the signal following the NI path. So far, we have considered that the first-order correlation function at the SLM plane was a Dirac delta. In order to take into account the effect of the finite size of the coherence length we can use a Gaussian-Schell model (GSM) to represent the first-order correlation function at the SLM plane [29],

$$G_0(u_1,u_2) = \exp\left[-\frac{u_1^2+u_2^2}{4\sigma^2} - \frac{(u_1-u_2)^2}{2\delta^2}\right]. \quad (12)$$

We have considered Gaussian apertures to represent the double-slit aperture,

$$A(u) = \exp\left[-\frac{(u-d/2)^2}{w_0^2}\right] + \exp\left[-\frac{(u+d/2)^2}{w_0^2}\right], \quad (13)$$

where the slit width is the FWHM of each of these Gaussians $a = 2w_0\sqrt{\ln 2}$ and d is the slit spacing. We have used the same values of the experiment for these parameters, $a = 0.25$ mm and $d = 0.45$ mm. The propagation of the first-order correlation function from the SLM to the CCD plane is given by Eq. (4). Using Gaussian apertures, the numerical evaluation of integrals in Eq. (4) converges more easily.

Figure 4 displays the simulations of the configuration without coordinate inversion. Figures 4(a) and 4(b) shows results for the first-order correlation function for $n = 2$ and $n = 4$, with $\alpha = 0.3$ mm, the same value used in the experiment. The values of the coherence length δ were 0.06, 0.2, 0.3, and 0.5 mm.

We noticed that changing the coherence length the pattern changes its height and width. These results show that, depending on the values of the coherence length, the phase aberration may not be completely canceled. The better cancellation occurs for smaller values of δ.

Figures 4(c) and 4(d) show the differences between the aberrated and nonaberrated first-order correlation curves D^{NI} as a function of the coherence length δ. Figure 4(c) shows D^{NI} as a function of δ for $n = 2$ and $n = 4$, using $\alpha = 0.3$ mm. The same was done in Fig. 4(d), but with $\alpha = 0.8$ mm. We observe that in Fig. 4(c) the differences are bigger for $n = 4$ than for $n = 2$, for values of coherence lengths smaller than $\delta = 0.2$ mm, and this behavior inverts for values bigger than that. However, this inversion does not occur for $\alpha = 0.8$ mm. To understand the last statements Table II displays some values for the phase aberration $\psi_n(x) = \pi(x/\alpha)^n$ and its variation $d\psi_n/dx = (n\pi/\alpha^n)(x)^{n-1}$ evaluated at the center of the slits, $x = \pm d/2$.

Using $\alpha = 0.3$ mm the slope of the phase aberration is bigger for $n = 4$ than for $n = 2$. This justifies the behavior

TABLE II. Phase aberration and its slope evaluated at the center of the slits.

	$\psi_n\left(\pm\frac{d}{2}\right)$	$\frac{d\psi_n}{dx}\big\|_{x=\pm d/2}$
$n = 2$ $\alpha = 0.3$ mm	1.8	± 15.7
$n = 4$ $\alpha = 0.3$ mm	1	± 17.7
$n = 2$ $\alpha = 0.8$ mm	0.2	± 2.2
$n = 4$ $\alpha = 0.8$ mm	0.02	± 0.3

observed in Fig. 4(c) for coherence lengths smaller than $\delta = 0.2$ mm. Bigger values for the difference parameter D^{NI} with $n = 4$ for these coherence lengths indicate that the effect is more sensitive to variations in the phase aberrations at these coherence lengths, but at $\delta = 0.2$ mm this behavior inverts. Above this point, the local values of the phase become more important than the variation. For $\alpha = 0.8$ mm, D^{NI} is always bigger than for $n = 2$ corresponding to the fact that these values of α and n imply bigger values of the phase and of its variation, than for $n = 4$. The main finding of this analysis is that, increasing the coherence, the overall phase cancellation becomes less effective resulting in the increased values of D^{NI}. Therefore, one should use the smallest possible coherence length in order to obtain the better aberration cancellation $D^{\mathrm{NI}} \ll 1$.

VI. CONCLUSION

Correlations of intensity fluctuations of far-field laser speckles were explored to show cancellation of aberrations. Unlike the quantum correlated twin-photons experiment, this method does not require coordinated inversion and works for any type of phase aberration.

It is important to note that once we showed how the aberration cancellation works, the configuration without phase aberration inversion in the signal beam path would not need a reference beam; all we would need would be to perform the autocorrelation. Additionally, the autocorrelation of the far-field scattered speckle pattern, Eq. (5), is proportional to the Fourier transform of the aperture with no aberrations, and it was already demonstrated that it is possible to recover an image from this autocorrelation function [21,22]. Therefore this effect can be useful for imaging in the presence of aberrations such as imaging through random media and microscopy.

ACKNOWLEDGMENTS

The authors acknowledge the financial support from the following agencies: Coordenação de Aperfeiçoamento de Pessoal de Nível Superior (CAPES); Conselho Nacional de Desenvolvimento Científico e Tecnológico (CNPq); Fundação de Amparo à Pesquisa do Estado de Alagoas (FAPEAL); Instituto Nacional de Ciência e Tecnologia de Informação Quântica (INCT-IQ).

[1] H. Gross, H. Zügge, M. Peschka, and F. Blechinger (Wiley-VCH Verlag GmbH & Co., Weinheim, Germany, 2007).
[2] A. M. Steinberg, P. G. Kwiat, and R. Y. Chiao, Phys. Rev. Lett. **68**, 2421 (1992).
[3] O. Minaeva, C. Bonato, B. E. A. Saleh, D. S. Simon, and A. V. Sergienko, Phys. Rev. Lett. **102**, 100504 (2009).
[4] V. Giovannetti, S. Lloyd, L. Maccone, and F. N. C. Wong, Phys. Rev. Lett. **87**, 117902 (2001).
[5] M. B. Nasr, B. E. A. Saleh, A. V. Sergienko, and M. C. Teich, Phys. Rev. Lett. **91**, 083601 (2003).
[6] C. Bonato, A. V. Sergienko, B. E. A. Saleh, S. Bonora, and P. Villoresi, Phys. Rev. Lett. **101**, 233603 (2008).
[7] D. S. Simon and A. V. Sergienko, Phys. Rev. A **82**, 023819 (2010).
[8] D. S. Simon and A. V. Sergienko, Opt. Express **18**, 9765 (2010).
[9] M. V. da Cunha Pereira, L. A. P. Filpi, and C. H. Monken, Phys. Rev. A **88**, 053836 (2013).
[10] C. J. Pugh, P. Kolenderski, C. Scarcella, A. Tosi, and T. Jennewein, Opt. Express **24**, 20947 (2016).
[11] L. A. Filpi, M. V. da Cunha Pereira, and C. H. Monken, Opt. Express **23**, 3841 (2015).
[12] K. J. Resch, P. Puvanathasan, J. S. Lundeen, M. W. Mitchell, and K. Bizheva, Opt. Express **15**, 8797 (2007).
[13] V. Torres-Company, H. Lajunen, and A. T. Friberg, New J. Phys. **11**, 063041 (2009).
[14] D. V. Strekalov, A. V. Sergienko, D. N. Klyshko, and Y. H. Shih, Phys. Rev. Lett. **74**, 3600 (1995).
[15] R. S. Bennink, S. J. Bentley, and R. W. Boyd, Phys. Rev. Lett. **89**, 113601 (2002).
[16] A. Valencia, G. Scarcelli, M. D'Angelo, and Y. Shih, Phys. Rev. Lett. **94**, 063601 (2005).
[17] T. Shirai, H. Kellock, T. Setälä, and A. T. Friberg, J. Opt. Soc. Am. A **29**, 1288 (2012).
[18] F. Wang, Y. Cai, and B. J. Hoenders, J. Opt. Soc. Am. A **31**, 48 (2014).
[19] C. R. Alves, A. J. Jesus-Silva, and E. J. S. Fonseca, Phys. Rev. A **93**, 043816 (2016).
[20] J. R. Fienup, Opt. Lett. **3**, 27 (1978).
[21] J. Bertolotti, E. G. van Putten, C. Blum, A. Lagendijk, W. L. Vos, and A. P. Mosk, Nature **491**, 232 (2012).
[22] J. A. Newman and K. J. Webb, Phys. Rev. Lett. **113**, 263903 (2014).
[23] C. R. Alves, A. J. Jesus-Silva, and E. J. S. Fonseca, Phys. Rev. A **94**, 013835 (2016).
[24] C. Dezhong, X. Jun, Z. Suheng, L. Lufang, G. Lu, and W. Kaige, Appl. Phys. Lett. **92**, 201102 (2008).
[25] I. Reed, IRE Trans. Inf. Theory **8**, 194 (1962).
[26] J. D. Gaskill, *Linear Systems, Fourier Transforms, and Optics*, Wiley Series in Pure and Applied Optics (Wiley, New York, 1978).
[27] B. E. A. Saleh, A. F. Abouraddy, A. V. Sergienko, and M. C. Teich, Phys. Rev. A **62**, 043816 (2000).
[28] A. Cao, A. K. Pandya, G. K. Serhatkulu, R. E. Weber, H. Dai, J. S. Thakur, V. M. Naik, R. Naik, G. W. Auner, R. Rabah *et al.*, J. Raman Spectrosc. **38**, 1199 (2007).
[29] L. Mandel and E. Wolf, *Optical Coherence and Quantum Optics* (Cambridge University Press, Cambridge, 1995).